Available online at www.sciencedirect.com
ScienceDirect
Polymer 48 (2007) 2969–2979
polymer
www.elsevier.com/locate/polymer

High improvement in the properties of exfoliated PU/clay nanocomposites by the alternative swelling process

Y.W. Chen-Yang [a,b,c,*], Y.K. Lee [a,b], Y.T. Chen [a,b], J.C. Wu [d]

[a] Department of Chemistry, Chung Yuan Christian University, 200 Chung-Pei Road, Chung-Li, Taoyuan County 32023, Taiwan, ROC
[b] Center for Nanotechnology, Chung Yuan Christian University, 200 Chung-Pei Road, Chung-Li, Taoyuan County 32023, Taiwan, ROC
[c] R&D Center for Membrane Technology, Chung Yuan Christian University, 200 Chung-Pei Road, Chung-Li, Taoyuan County 32023, Taiwan, ROC
[d] Department of Chemical Engineering, Chung Yuan Christian University, 200 Chung-Pei Road, Chung-Li, Taoyuan County 32023, Taiwan, ROC

Received 2 October 2006; received in revised form 11 February 2007; accepted 6 March 2007
Available online 14 March 2007

Abstract

In this work, a stable de-aggregated solvent-swollen organic modified clay, ALA−MMT, suspension is prepared by an efficient solvent swelling process using a home-made shaking mixer. It is found that the estimated average size of the as-prepared organoclay particles in the suspension is reduced to about 155 nm, which has not been reported before. The X-ray diffraction (XRD) patterns confirm that the *d*-spacing of the silicate layers of the solvent-swollen ALA−MMT expands from 1.4 nm to about 2.1 nm. The de-aggregated solvent-swollen ALA−MMT suspension is then used with polyurethane (PU) to prepare a series of highly exfoliated and high-organoclay-loading nanocomposites, PU/ALA−MMT. Both the XRD patterns and the TEM photographs of the as-prepared PU/ALA−MMT nanocomposites indicate that the organoclay is uniformly dispersed in the PU matrix with a highly exfoliated morphology structure of up to 7 wt% loading. Meanwhile, the TEM photographs give the first report for PU/clay nanocomposites which are almost completely exfoliated, and ~1-nm thin silicate nanolayers are homogeneously dispersed in the polymer matrix with a high aspect ratio of 30−100. The thermal, mechanical, and anti-corrosion properties are all tremendously enhanced for the as-prepared nanocomposites. The results obtained for the PU nanocomposite with 7 wt% ALA−MMT loading (PUC7) reveal a 19 °C increment in T_g, a 48 °C increment in $T_{5\%}$, a 248% increase in the tensile strength, and a 123% increase in the elongation. The stainless steel disk (SSD) coated with PUC7 shows the lowest corrosion rate of 2.01×10^{-6} mm/year, which is 469% lower than that of the SSD coated with pure PU. The reinforcements are much greater than the previously reported PU/clay nanocomposites with comparable clay loadings ascribed to the exceptional homogeneity of as-prepared nanocomposites, which are accredited largely to the stable de-aggregated solvent-swollen organoclay suspension generated by the efficient solvent swelling process.

Keywords: Polyurethane; Clay; Nanocomposite

1. Introduction

In recent years, research in organic−inorganic nanocomposites has become popular, particularly in developing new polymer nanocomposites [1−4]. Montmorillonite (MMT) is one of the most promising layered silicate clays used as the inorganic filler for the preparation of nanocomposites, due to its high aspect ratio and natural abundance [5−7]. In addition to these features, the interlayer regions of MMT have Na^+, K^+, or Ca^{2+} ions which can be replaced via cationic exchanging by organic cations such as alkylammonium, making the silicate layer organophilic and compatible with organic polymers. Many polymer/organoclay nanocomposite materials such as polycaprolactone/organoclay [8], polystyrene/organoclay [9,10], epoxy/organoclay [11−14], polyimide/organoclay [15,16],

* Corresponding author. Department of Chemistry, Chung Yuan Christian University, 200 Chung-Pei Road, Chung-Li, Taoyuan County 32023, Taiwan, ROC. Tel.: +886 3 2653317; fax: +886 3 2653399.
E-mail address: yuiwhei@cycu.edu.tw (Y.W. Chen-Yang).

0032-3861/$ - see front matter © 2007 Elsevier Ltd. All rights reserved.
doi:10.1016/j.polymer.2007.03.024

and polymethylmethacrylate/organoclay [17–19] systems have been reported. In general, by dispersing a small amount of nano-scaled clay as an inorganic filler in a polymer matrix, the mechanical, dimensional, thermal, and barrier performance properties of the formed organic–inorganic nanocomposites were significantly enhanced.

Polyurethanes (PUs) are known as a very useful material in industrial applications due to their good biocompatibility, excellent abrasion resistance, and flexural fatigue characteristics. Similar to other common polymers, several PU/organoclay nanocomposites have been studied by different groups [20–35]. The effect of the addition of organoclays on property improvement is related to the morphology structure and the dispersion efficiency of the organoclay particles in the polymer matrix, which is associated with the compatibility between the polymer and the organoclay. Generally, in order to improve compatibility, the swelling agents with similar hydrophobicity property as the polymer were selected to modify the original clays. Moreover, the organoclays containing reactive end-groups, such as hydroxyl group, were also prepared and used as an extender in the formation of PU/organoclay nanocomposites. Furthermore, in previous studies, PU/organoclay nanocomposites were prepared either by conventional stirring of the organoclay with the polymers or by in situ polymerization of the monomers or prepolymers [1,20–25,30–35]. It was found that compared with those of pristine PU, the physical properties of the as-prepared organoclay-containing PU nanocomposites were enhanced when the orgnoclay loading was increased up to about 1 wt%, but deteriorated as the organoclay loading exceeded 1 wt% due to the aggregation of organoclay. In these studies, both the XRD and TEM results of the nanocomposites indicated that the organoclay particles were mainly are intercalated structures with nanolayers stacked in a crystallographic order in the polymer matrix [26–28]. This indicates that aggregation could not be prevented by the conventional stirring method, and de-aggregation is important for the further improvement of the properties of nanocomposites when the clay-loading is increased.

Our goal in this study is to provide a PU-compatible, less-aggregated, and organic modified MMT suspension in order to prepare highly exfoliated and homogeneously dispersed PU/organoclay nanocomposites with high-organoclay-loading to largely enhance their properties. Therefore, a reactive organophilic montmorillonite, ALA–MMT, obtained by modifying MMT with 12-aminodecanoic acid (ALA), a mono-functional reactive group-containing long-chain-alkylammonium swelling agent, was selected. In addition, a home-made shaker was also used to quickly de-aggregate the organoclay in the solvent, reducing the particle size and further expanding the silicate layers to obtain a stable suspension. The dispersion morphology and the corresponding particle size of the organoclay, ALA–MMT, in the solvent were analyzed by the XRD patterns and the particle size analyzer, respectively. The dispersion morphology in the as-prepared PU/ALA–MMT nanocomposites was studied by the XRD and TEM measurements. The thermal, mechanical, and anti-corrosion properties of the PU/ALA–MMT nanocomposites were also investigated to confirm the function of clay-loading.

2. Experimental procedure

2.1. Materials

PK-805, a Na^+-montmorillonite with a cation-exchange capacity of 98 mequiv/100 g, was obtained from Paikong Ceramic Company (Taiwan). Basically, 12-aminodecanoic acid (12-aminolauric acid, ALA), the swelling agent, and polypropylene glycol (PPG, $M_n = 2000$) were purchased from TCI company (Japan). Also, 1-isocyanato-4-[(4-isocyanatophenyl)methyl]benzene (MDI), 1,4-butanediol (1,4-BD), and *N*,*N*-dimethylformamide (DMF) were purchased from Acros Chemical Company. Prior to usage, PPG and 1,4-BD were dehydrated under vacuum in an oven at 80 °C, while DMF was dried over calcium hydride for 2 days, and MDI was melted under N_2 at 80 °C.

2.2. Preparation of organoclay, ALA–MMT

The organophilic montmorillonite, also referred to as ALA–MMT, was obtained through a multi-step process as follows [25,28–30,32]. First, 40.0 g of PK-805, a Na^+-montmorillonite clay (MMT), was dispersed in 4.0 l of distilled water with vigorous mechanical stirring to form a uniformly suspended solution. In a 500 ml beaker, 10.0 g of ALA was mixed with 10 ml of concentrated HCl and 300 ml of water to form an ammonium salt. The ALA ammonium salt solution was added to the MMT suspended solution and stirred vigorously at 80 °C overnight to carry out the cationic exchange. The modified MMT was collected by employing the centrifugal process, and it was repeatedly washed with de-ionized water to ensure the complete removal of chloride ions until no AgCl precipitate was observed to titrate the filtrate with 0.1 N $AgNO_3$. The modified clays were then dried at 100 °C in a vacuum oven for 24 h. The ALA–MMT was finally hand-grounded and screened with a 325 mesh sieve. The yield of ALA–MMT obtained by this method was about 90%.

2.3. Synthesis of pure PU

The preparation procedure for the polyurethane film is shown in Scheme 1. A 52.5 ml of DMF solution containing 10.0 g (5.0 mmol) of PPG and 7.5 g (30.0 mmol) of MDI was added to a dry 250 ml two-necked flask equipped with nitrogen inlet. Then the solution was refluxed under magnetic stirring at 80 °C for 2 h to form the PU prepolymer. A solution of 1.8 g (25.0 mmol) of 1,4-BD in 6.8 ml of DMF was added into the prepolymer solution and was stirred for another 2 h. This reaction mixture was cooled to room temperature and further stirred for another 2 h. The as-prepared viscous solution was then cast onto a glass plate and dried in an oven at 80 °C for 1 day to further polymerization and remove the solvent. The final thin film formed was about 0.5 mm thick.

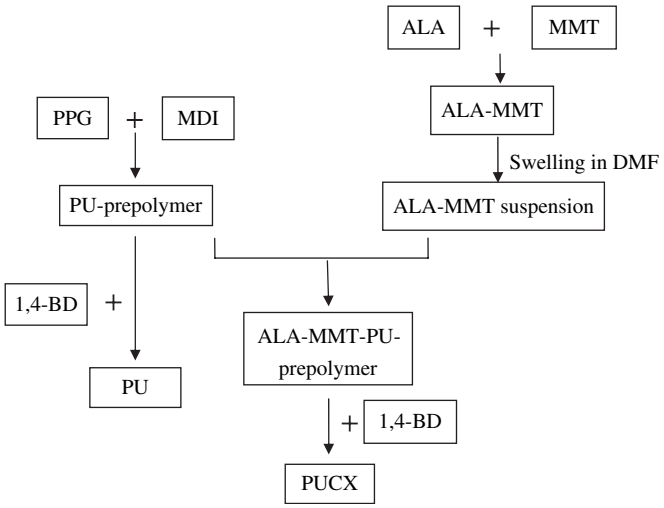

Scheme 1. The preparation procedure of PU/ALA–MMT nanocomposites.

2.4. Synthesis of PU/ALA–MMT nanocomposites, PUCX

To prepare PU/ALA–MMT nanocomposites (PUC*X*) (as shown in Scheme 1), first, the various amounts (1, 3, 5 or 7 wt%) of ALA–MMT organoclay were shaken for 20–60 min with the home-made shaker to form the ALA–MMT suspensions. The PU-prepolymer solution, synthesized as that for pure PU, was added into the ALA–MMT suspensions and stirred for 2 h to form the corresponding ALA–MMT–PU prepolymer solutions. Then the designated amount of extender, 1,4-BD, was added into the ALA–MMT–PU prepolymer solution and stirred for another 2 h to form a viscous solution. Similar to the pure PU film, the individual PUC*X* film was prepared by casting the as-prepared viscous solution onto a glass plate. Consequently, the solution was dried in an oven for 1 day at 80 °C to complete the polymerization reaction and remove the solvent.

2.5. Instrumentation

The mixer used for the organoclay suspension was a home-made shaker (model SH-15A), which was assembled by fixing a wine-shaker bottle as the sample holder in an automatic-controlled shaker. The shaking frequency of the shaker was 300 times/min. The ATR spectra were taken on a Bio-Rad FTS-7 system with a wave number resolution of 4 cm^{-1} within the range of 500–4000 cm^{-1} (film). The X-ray diffraction (XRD) experiments of the samples were performed from 1° to 10° at a scanning rate of 1°/min using a Siemens D5000 X-ray diffractometer. The X-ray beam was generated from the nickel-filtered Cu Kα ($\lambda = 1.54$ Å) radiation in a sealed tube operated at 50 kV and 25 mA. The samples for the transmission electron microscopic (TEM) study were first microtomed with Leica Ultracut Uct into about 70-nm thick slices at −80 °C and then were measured with a TEM model JOEL-2000 FX STEM (Japan). The differential scanning calorimetric (DSC) analysis was conducted with a SEIKO DSC-220 analyzer (Japan) from −100 °C to 100 °C at a heating rate of 10 °C/min under a nitrogen purge. The thermal gravimetric analysis (TGA) was carried out from 30 °C to 600 °C by a SEIKO TG/DTA 220 (Japan) thermal analyzer at a heating rate of 20 °C/min. The tensile strength tests were carried out according to ASTM D882 by HT-9101 of the Universal Tensile Testing Instrument Company. The tester was equipped with a 500 N load cell and interfaced to a computer for data collection. The sample sizes were 100 mm × 10 mm, which include 40 mm long clipped parts (20 mm at each end) and the crosshead speed was set at 500 mm/min. The particle size of the organoclay suspended in DMF was estimated by a light scattering particle size analyzer (BROOKHAVEN 90 PLUS). The anti-corrosion properties of the PU/organoclay nanocomposite coatings on the stainless steel disks (SSDs) were evaluated by the Tafel method. All the electrochemical measurements of the sample-coated SSD coupons were performed on an Autolab PGSTAT3 in a standard corrosion cell equipped with two graphite counter electrodes and a saturated calomel electrode as reference, as well as the working electrode at room temperature. The Tafel plots were obtained by scanning potential from below 250 mV to above 250 mV of the corrosion potential, E_{corr}, at a scanning rate of 600 mV/min.

3. Results and discussion

3.1. Characterization of organoclay, ALA–MMT

The structure of ALA–MMT is studied by the XRD and FTIR measurements. As reported previously [29], the montmorillonite, MMT, had a characteristic diffraction peak at $2\theta = 7.0°$, indicating that the *d*-spacing of the silicate layers was about 1.2 nm. As indicated in Fig. 1, the characteristic peak of the silicate layers in ALA–MMT was shifted to $2\theta = 6.3°$, corresponding to an interlayer distance of 1.4 nm. This reveals that the layer galleries of MMT were expanded due to the modification of ALA, which contained a long-chain

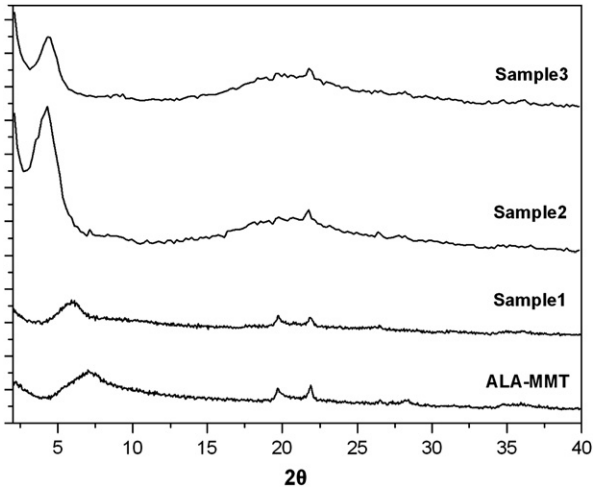

Fig. 1. XRD patterns of the precipitates of the ALA–MMT suspension in DMF after centrifugation.

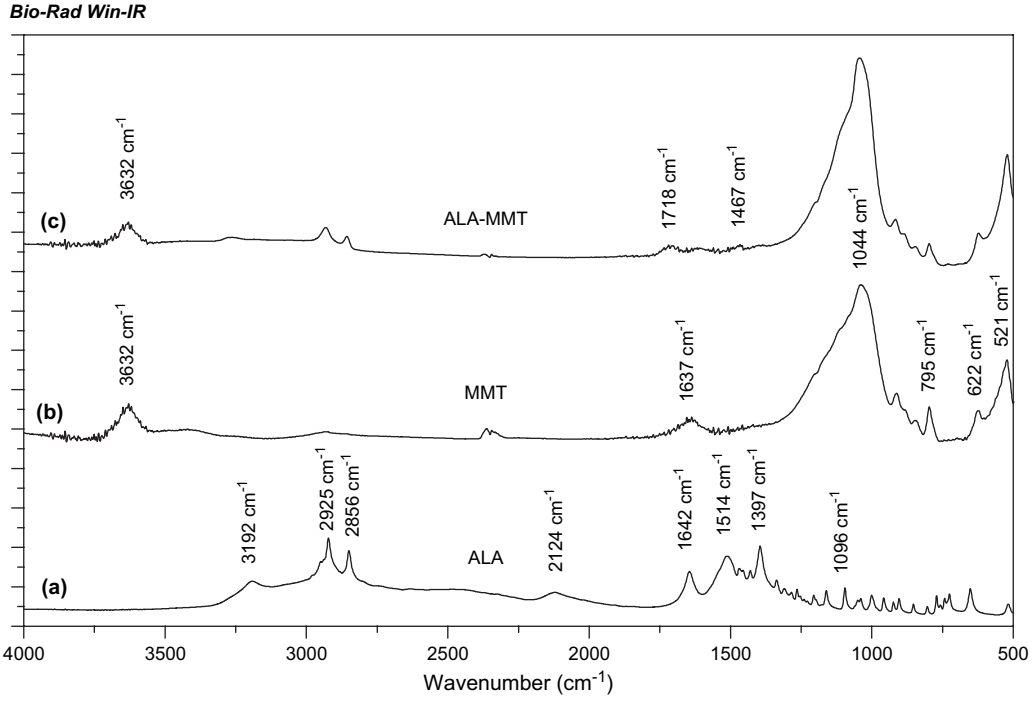

Fig. 2. FTIR spectra of (a) ALA, (b) MMT, and (c) ALA–MMT.

alkyl group. However, the ordered structure of the clay layers still remained.

The FTIR spectra of MMT, ALA, and ALA–MMT are shown in Fig. 2. As can be seen in Fig. 2(a), the characteristic absorptions of ALA were found at 3192 cm^{-1} (N–H stretching), 2925 cm^{-1} (C–H asymmetric stretching), 2856 cm^{-1} (C–H symmetric stretching), 1642 cm^{-1} (O–H bending and N–H deformation), and 1096 cm^{-1} (C–N stretching). Especially, the strong absorptions peaked at 1514 cm^{-1} and 1397 cm^{-1} for asymmetric stretching and symmetric stretching of the R–COO^- group and at 2124 cm^{-1} for the absorptions of combination bonds of COO^- and N–H stretching indicated that the carboxylic group of ALA was in dissociated form. From Fig. 2(b), the characteristic absorptions at 3632 cm^{-1} (O–H stretching), 1044 cm^{-1} (Si–O in-plane stretching), 795 cm^{-1} (Si–O stretching), 622 cm^{-1} (coupled Al–O and Si–O out-of-plane vibration), and 521 cm^{-1} (Al–O–Si deformation) as well as the weak broad absorption between 3531 cm^{-1} and 3233 cm^{-1} (H–OH hydrogen bonded water) and at 1637 cm^{-1} (O–H deformation of entrapped water) were observed for the dried MMT. In addition, as shown in Fig. 2(c), the FTIR features of ALA–MMT were mainly a combination of characteristic absorptions of MMT and ALA. The absorptions in the range of 1300 cm^{-1} and 500 cm^{-1} and that at 3632 cm^{-1} were almost identical to that of MMT, indicating that the main structure of the silicate layer was unchanged. On the other hand, the disappearance of absorption between 3531 cm^{-1} and 3233 cm^{-1} of bonded water, and the appearance of the absorption in the region of 3317–3154 cm^{-1} assigned to the ionic bonded N–H stretching vibration of N^+H_3 showed the evidence that the interlayer water was replaced by ALA by cationic exchange. Besides, the appearance of the absorptions at 1718 cm^{-1} for C=O stretching and that at 1467 cm^{-1} for CO–H bending revealed the presence of the hydrogen bonded COOH group, which also confirmed that the COOH of ALA was protonated into the protonated form in ALA–MMT by the hydrochloric acid. The absence of the characteristic absorption of ester C=O between 1735 cm^{-1} and 1750 cm^{-1} revealed that the esterification between COOH of ALA and –OH groups on platelet edge of MMT did not occur in the cationic exchange reaction. The result confirms that most of the amino and carboxylic groups of ALA were protonated by hydrochloric acid into N^+H_3 and COOH, respectively, and remained in the protonated forms in ALA–MMT after ionic exchange as reported by Katti et al. [36].

3.2. Preparation of stable de-aggregated solvent-swollen ALA–MMT suspension

As mentioned earlier, aggregation is usually found in the clay-containing PU nanocomposites when the organoclay-loading exceeds 1 wt% [20–35]. In this study, the aggregation was thought to have occurred before the organoclay solution was mixed with the PU polymer or the PU prepolymer. Therefore, if the organoclay could be de-aggregated into particles of smaller size in the solvent, and the *d*-spacing of the silicate layers can be further enlarged, the dispersion efficiency of the organoclay in the PU matrix would be effectively increased even while the loading increased, resulting in high enhancement of the properties of the nanocomposites. In order to achieve this purpose, instead of the conventional method of

stirring magnetically in one direction, an effective mixing process of shaking the solution back and forth was performed with a home-made shaker in DMF to prepare the stable ALA–MMT suspensions. It was found that with 2 h of conventional magnetic stirring, the ALA–MMT organoclay (Sample 1) was initially suspended in the DMF solution. However, as indicated in Table 1, after allowing to stand for a day, the lower 25% part of the solution of the ALA–MMT was precipitated, indicating that the size of the particles was not de-aggregated enough to suspend in the solution. For Sample 2, after being shaken for 20 min by the shaker, the precipitation phenomenon was also found, but the height of the precipitate was increased to about 40% of the solution, revealing that de-aggregation was more effectively achieved by the shaking process than by the magnetic stirring method. As the shaking time was increased to 60 min, stable suspension, Sample 3, was obtained. This implies that the organoclay particles in the sample were small enough to suspend in DMF for a day. To confirm the reduction of particle size by the shaking process, the particle sizes of the ALA–MMT organoclays of the suspensions were estimated by the light scattering particle size analyzer, which is known mainly for the measurement of spherical particle suspension. Since the clay particles were not in spherical form, the result of the measurements was used only for obtaining the relative trend of the particle sizes in the as-prepared suspensions. The average size of the organoclay particles of Sample 1 was about 1.6 μm. With the shaking process, the estimated average size of the organoclay particles in the suspension was reduced to about 155 nm for Sample 3, which was only about 1/10 of the original average size. This indicates that the shaking process effectively de-aggregated the ALA–MMT clay in the DMF solution, giving stable suspension within 1 h. The successful de-aggregation is ascribed to the shearing force provided by the shaking process.

In addition, the XRD patterns (Fig. 1) of the ALA–MMT suspended samples obtained by high-speed centrifugation showed that the characteristic peaks shifted from $2\theta = 6.3^\circ$ to about 5.8° for the magnetically stirred Sample 1, and 4.2° for the shaken Samples 2 and 3, corresponding to the *d*-spacing of approximately 1.5 nm and 2.1 nm, respectively. This implies that with a short time shaking (<1 h), the *d*-spacing of the ordered clay layers was expanded from 1.4 nm of the pristine ALA–MMT sample to approximately 2.1 nm in the DMF suspension. The enlargement is ascribed to the efficient solvent swelling by DMF due to the compatibility with the organoclay and the small size of the particles.

Table 1
The height of the precipitate of ALA–MMT in DMF solution after mixing

Sample number	Mixing method	Mixing time (min)	% Height of the solution[a] (%)	Particle size (nm)
1	Magnetic stirring	120	25	1558
2	Shaking	20	40	858
3	Shaking	60	100 (stable suspension)	155

[a] Measured after standing for a day.

3.3. Morphology and dispersion of ALA–MMT in PU/ALA–MMT nanocomposites

The XRD patterns of the PU/ALA–MMT nanocomposites (PUC*X*, where *X* represents the wt% of ALA–MMT loading) are presented in Fig. 3. As can be seen, the diffraction peak of ALA–MMT is almost invisible in the patterns for PUC1 and PUC3 and very weak for PUC5 and PUC7. This reveals that only a very few ordered ALA–MMT remained, and majority of the silicate layers of the organoclay were either intercalated to a space of more than 8.8 nm ($2\theta < 1^\circ$) or completely exfoliated by the PU chains. For instance, a high degree of exfoliation was achieved in all these PU nanocomposites even for an extra 7 wt% of ALA–MMT.

More direct evidences of the formation of a true nanocomposite were provided by TEM investigation. Fig. 4 shows the TEM micrographs at low and high magnitude for the nanocomposites. The low magnitude micrographs confirm that the clay particles were well-dispersed in the PU matrix, and the ones with high magnitude showed that the clay layers were dispersed at the monolayer level. The dark lines in the figures are the intersections of the clay sheets, and the spaces between the dark lines are the interlayer spaces. As can be seen, most of the silicate layers were completely exfoliated into about 1-nm thick nanolayers to an extent of 30–100 nm, i.e., the layers were in molecularly thin sheets with a high aspect ratio. Unlike previous reports [20–35] for the PU/clay nanocomposites, which showed a high percentage of intercalated structures, the result confirms that the ALA–MMT nanolayers were homogeneously dispersed in the PU matrix with a highly exfoliated structure in the as-prepared PU/ALA–MMT nanocomposites. To our best knowledge, there was no TEM photograph for the PU/clay nanocomposite ever reported with such homogeneous clay dispersion and high degree of exfoliation. Moreover, this result was consistent with the XRD result concluded earlier.

Compared with the results reported [26–28] in which the clay solution with micro-scale clay particles was prepared by conventional stirring or sonication process, evidently, the

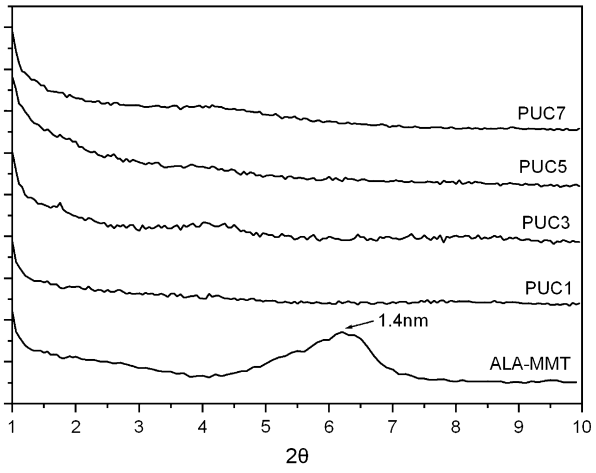

Fig. 3. X-ray diffraction patterns of PU/ALA–MMT nanocomposites (PUC*X*).

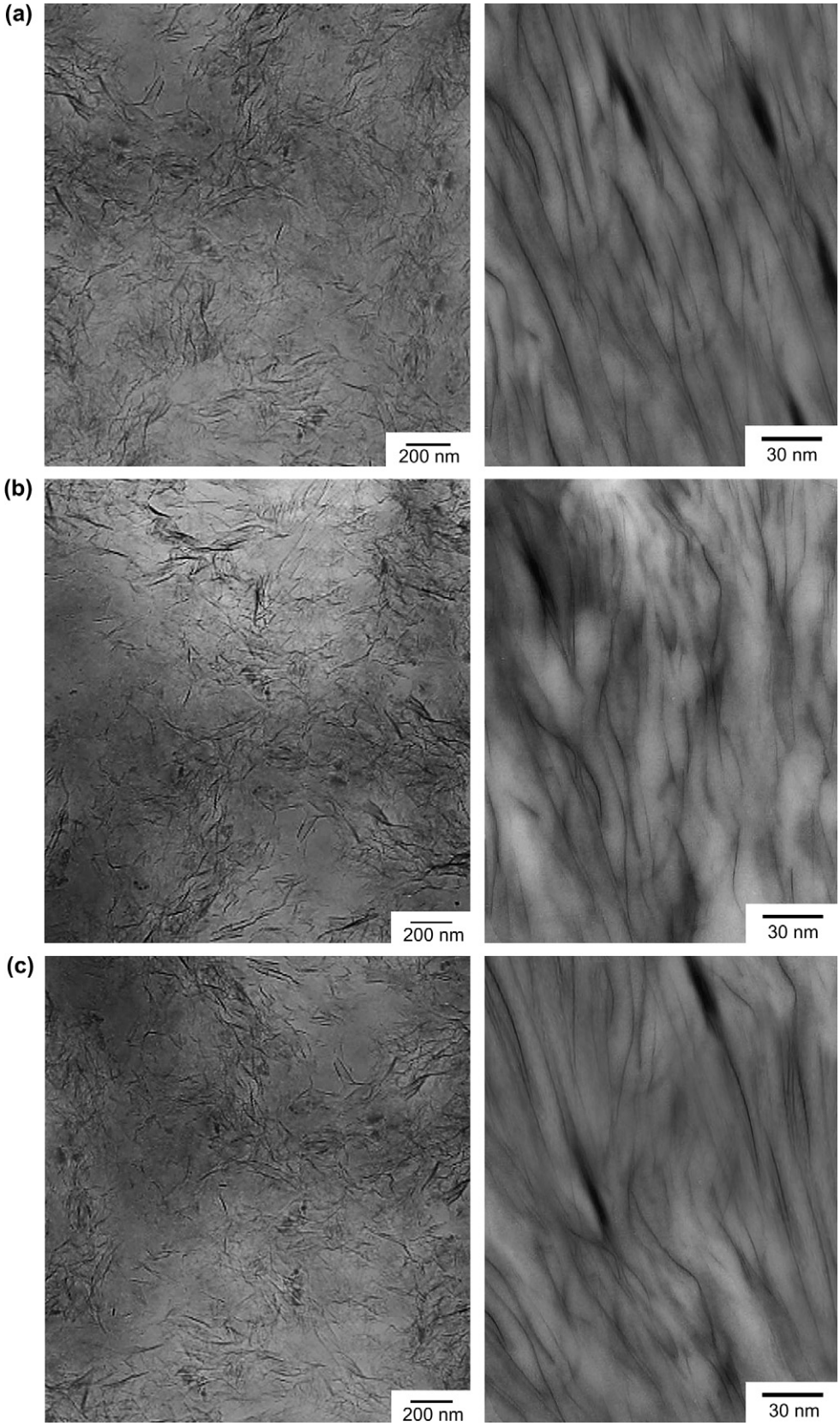

Fig. 4. TEM photograph of PU/ALA–MMT nanocomposites (a) PUC3, (b) PUC5, and (c) PUC7.

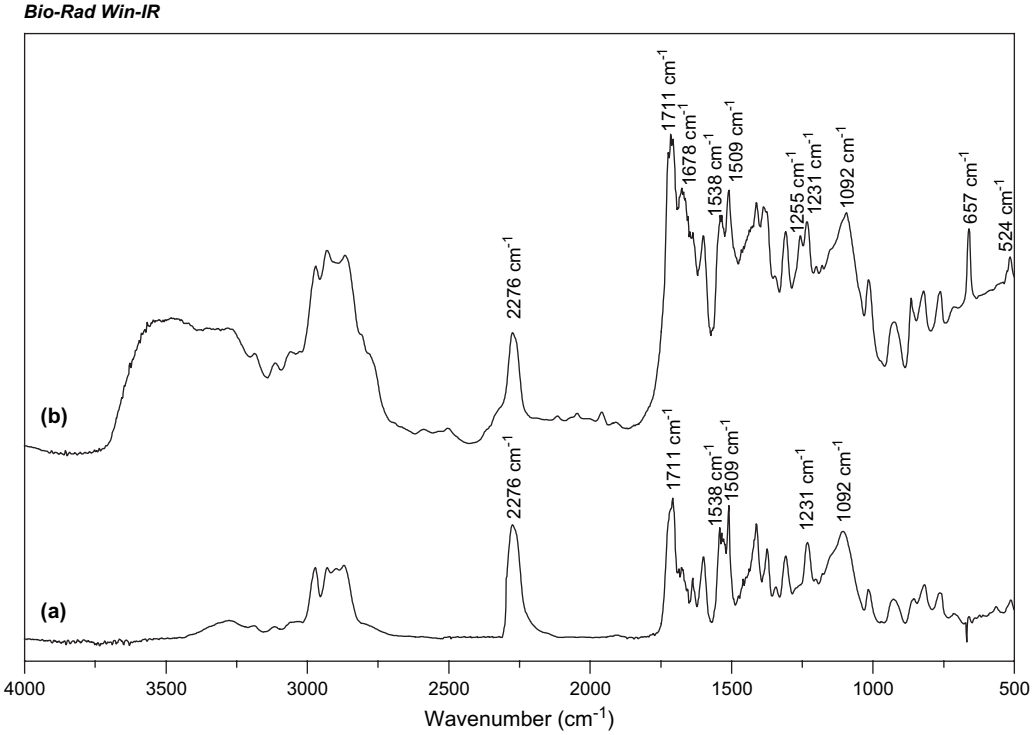

Fig. 5. FTIR spectra of (a) the NCO-terminated PU prepolymer and (b) the NCO-terminated ALA−MMT−PU prepolymer.

extremely high exfoliation morphology and the homogeneous clay dispersion of the PU nanocomposites prepared in this study are attributed to the successful preparation of the stable de-aggregated solvent-swollen ALA−MMT suspension and the ALA−MMT−PU prepolymer. The advantage of the shaking process over the stirring one is ascribed to the higher probability of collision between particles during shaking than stirring. During stirring, all the particles go around in the same direction, whereas during shaking, the continuous change in direction of the liquid movement causes more particle collisions and induces shearing force, which can assist the delamination of silicate platelets and the swelling of the solvent.

In order to know the possible reactions that occurred between ALA−MMT and the PU matrix in the nanocomposites, which include the reaction of isocyanate with the carboxylic group, the amine group of ALA or with any amine group formed by hydrolysis of isocyanate, the FTIR spectra of the NCO-terminated PU prepolymer and the NCO-terminated ALA−MMT−PU prepolymer were measured as shown in Fig. 5. Also, as seen in Fig. 5(a), the characteristic absorptions of the NCO-terminated PU prepolymer were observed at 2276 cm^{-1} (−N═C═O asymmetric stretching), 1711 cm^{-1} (C═O stretching of *N*-aryl urethane), 1538 cm^{-1} (CHN vibration), 1509 cm^{-1} (in-plane N−H bending), 1231 cm^{-1} (coupled C−N and C−O stretching), and 1092 cm^{-1} (C−O stretching). Comparing with Fig. 5(a), it can be seen in Fig. 5(b) that all the characteristic absorptions of the NCO-terminated PU prepolymer remained unchanged in the NCO-terminated ALA−MMT−PU prepolymer. Besides, the characteristic absorption of the silicate of MMT was observed at 524 cm^{-1} (Al−O−Si deformation) and 1044 cm^{-1} (Si−O in-plane stretching), which overlapped with that of 1092 cm^{-1} (C−O stretching of urethane). Furthermore, the extra absorption peaks at 3700−3400 cm^{-1} (N−H stretching), 1678 cm^{-1} (C═O stretching of amide), 1255 cm^{-1} (amide II vibration), and 657 cm^{-1} (O═C−N bending of amide group) indicated the formation of amide structure between ALA−MMT and the PU prepolymer to form the NCO-terminated ALA−MMT−PU prepolymer. This also revealed that enough terminal-COOH groups were provided by the ALA−MMT particles to react with the isocyanate groups of the PU prepolymers to form the amide groups, as depicted in Scheme 2. Evidently, the successful preparation of the de-aggregated solvent-swollen ALA−MMT nano-particles, which provided large surface area, was crucial to ensure the availability of enough terminal-COOH groups. Consequently, the ALA−MMT particles were homogeneously grafted onto the ALA−MMT−PU prepolymer through the formation of the amide groups, resulting in the proper dispersion of the ALA−MMT clay in the PU matrix of the as-prepared PU/ALA−MMT nanocomposites.

In addition, although the bands such as those at 1635 cm^{-1} could be due to the stretching of carbonyl groups of urea functionality formed by the reaction of isocyanate with amine groups, since the strong characteristic absorption of asymmetric stretching vibration of N−C−N group for urea was not found between 1490 cm^{-1} and −465 cm^{-1}, it is believed that no urea segments were formed in the ALA−MMT−PU prepolymer. This also indirectly supports that the amino groups of ALA in ALA−MMT are in protonated form,

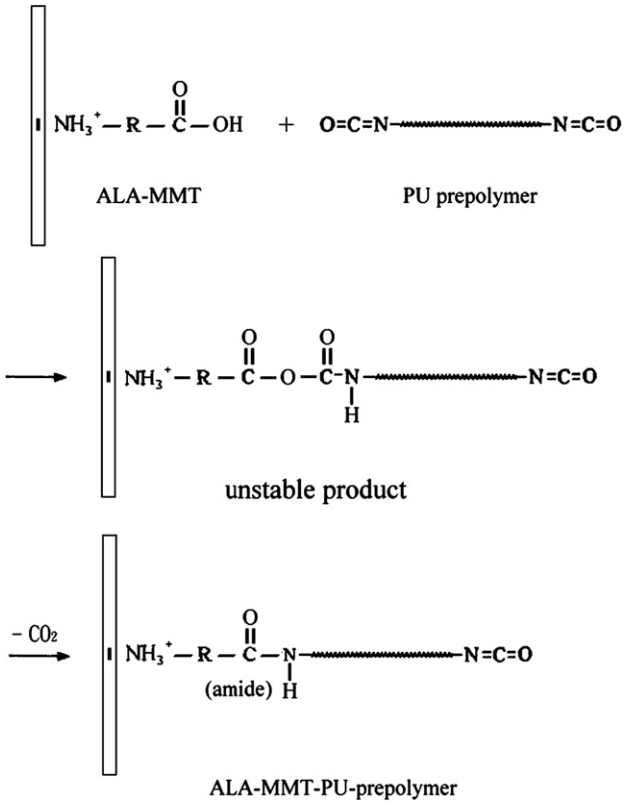

Scheme 2. Reaction of isocyanate with a carboxylic acid.

N^+H_3, attached to the silicate layers via the cationic exchange. It also reveals that the esterification did not occur in the cationic exchange reaction.

The chemical structures of the PU/ALA−MMT nanocomposites were also identified by ATR measurements. As seen in Fig. 6, the ATR spectrum of the pure PU shows that the characteristic bands for the N−H stretching, C−H stretching, C═O stretching, coupled C−O and C−N vibrations, and C−O vibration are observed at 3338 cm^{-1}, 2800−3000 cm^{-1}, 1716 cm^{-1}, 1255 cm^{-1}, and 1000−1107 cm^{-1}, respectively. The characteristic bands of the ALA−MMT structure are observed in the spectra of the PU/ALA−MMT nanocomposites at 524 cm^{-1} for the Al−O vibration and 1044 cm^{-1} for the Si−O vibration, which overlap with the peak of the C−O vibrations. As expected, the intensities of the characteristic peaks of ALA−MMT increased with increasing ALA−MMT loading. However, except for the absorption of the O═C−N bending at 665 cm^{-1}, the peaks of carbonyl and N−H stretching vibrations of the amide groups formed in the ALA−MMT−PU prepolymers were not observed for the PU/ALA−MMT nanocomposites as they overlapped with those of the urethane groups.

3.4. Thermal properties of PU/ALA−MMT nanocomposites

The DSC and TGA analyses were employed to investigate the thermal properties of the pure PU and the PU/ALA−MMT nanocomposites. As seen in Fig. 7, no melting peak was found in the DSC thermograms of the pure PU sample. This finding indicates that no crystallization domain has been formed in the hard segment phases, though a glass transition temperature, T_g, was observed for the soft segment phases of all the samples. Table 2 shows that the T_g of pure PU was −61.4 °C, which is very different from the T_gs of the PU/ALA−MMT nanocomposites. An abrupt T_g increase of 9 °C was measured for PUC1, the composite with only 1 wt%-organoclay. This

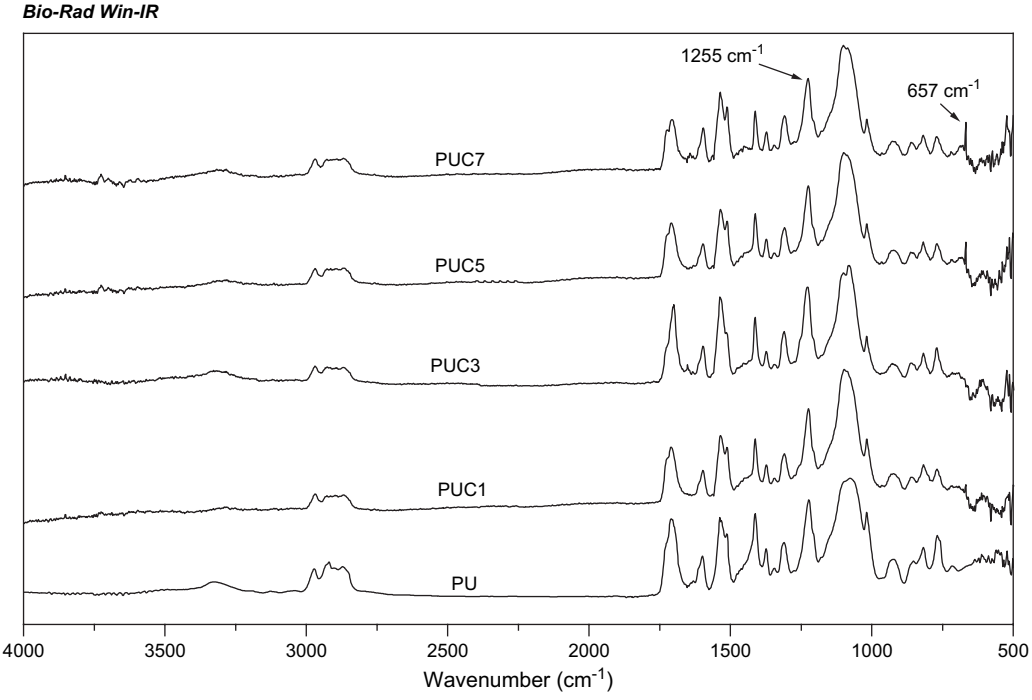

Fig. 6. ATR of the PU/ALA−MMT nanocomposites (PUC*X*).

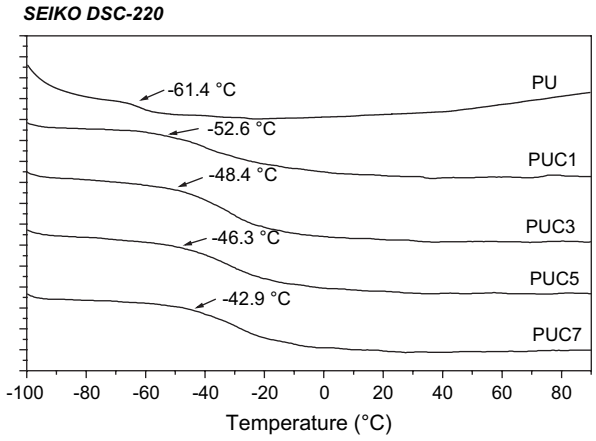

Fig. 7. DSC thermograms of PU/ALA–MMT nanocomposites (PUC*X*).

finding is discrepant with previous reports [20–23,29], in which the PU/clay composites with 1 wt%-organoclay and pure PU were found to have similar T_g's. In addition, the T_g was further increased by increasing the organoclay contents and PUC7, which contained 7 wt% of ALA–MMT, received a 19 °C increment to −42.9 °C. These indicate that the presence of ALA–MMT clay effectively retarded the glass transition of the as-prepared PU/ALA–MMT nanocomposites. The result is attributed to the decreased mobility of the polymer chains caused by the ALA–MMT which acted as a chain extender. This again supports that even for 7-wt% clay loading, the exfoliated clay layers were homogeneously grafted onto the PU matrix through the amide group formed from the solvent-swollen ALA–MMT nano-particles and the PU prepolymer.

The effects of ALA–MMT loading on the decomposition behavior were determined by TGA thermograms of the pure PU and the PU/ALA–MMT nanocomposites as shown in Fig. 8 and its corresponding data are given in Table 2. As indicated in the figure, the initial degradation temperature at 5 wt% weight losses ($T_{5\%}$) was at 280 °C for pure PU, which dramatically increased to 318 °C for PUC1. This $T_{5\%}$ temperature further jumped to 329 °C for PUC7. In addition, the maximum degradation temperature (T_{max}) of the nanocomposites also increased with increasing organoclay loading. For the nanocomposite with 1 wt% of organoclay, PUC1, the T_{max} was increased to 38 °C (from 375 °C to 412 °C), and the largest increase was 55 °C (from 375 °C to 430 °C) for PUC7. Compared with the pure PU, the nanocomposites in

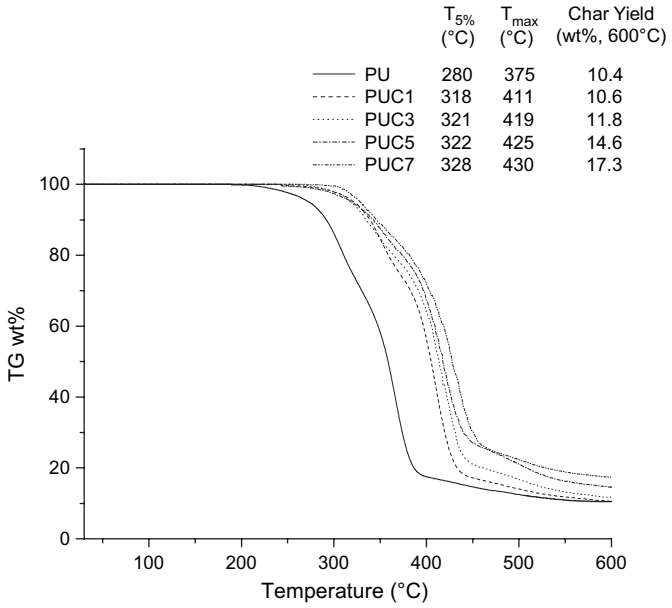

Fig. 8. TGA thermograms of PU/ALA–MMT nanocomposites (PUC*X*).

this study exhibited a delayed decomposition, and the thermal stability was largely improved by the presence of the dispersed organoclay. The increase in thermal stability is attributed to the good thermal stability of the well-dispersed and exfoliated silicate layers of the organoclay. Since all the silicates of the organoclay in the as-prepared nanocomposites had highly exfoliated structure, the number of exfoliated platelets increased correspondently with the increasing organoclay loading. Therefore, the retardant effect of the exfoliated silicate layers on heat diffusion in the PU matrix was strengthened in the nanocomposite.

Table 2 also shows the increases of 10.6% to 17.3% of the char residue at 600 °C as the clay contents increased from 1 wt% to 7 wt%. This observation suggests that the flame retardancy of the nanocomposite can also be enhanced by increasing the ALA–MMT loading due to the protection of oxygen diffusion by the char residue formed on the surface.

3.5. Mechanical properties of PU/ALA–MMT nanocomposites

The detailed tensile mechanical properties of the PU/ALA–MMT nanocomposites with different organoclay contents are summarized in Table 3. It shows that the presence

Table 2
The thermal data of the PU/ALA–MMT nanocomposites (PUC*X*)

PUC*X* sample	ALA–MMT content (wt%)	$T_{5\%}$ (°C)	$\Delta T_{5\%}$[a] (°C)	T_{max} (°C)	ΔT_{max}[a] (°C)	Char yield at 600 °C (wt%)	ΔChar yield[a] at 600 °C (wt%)	T_g (°C)	ΔT_g[a] (°C)
PU	0	280	–	375	–	10.4	–	−61.4	–
PUC1	1	319	+38	412	+36	10.6	+0.2	−52.6	+9
PUC3	3	321	+41	420	+44	11.8	+1.4	−48.4	+13
PUC5	5	323	+43	425	+50	14.6	+4.2	−46.3	+15
PUC7	7	328	+48	430	+55	17.3	+6.9	−42.9	+19

[a] Compared with the pure PU's data.

Table 3
Mechanical properties of the PU/ALA–MMT nanocomposites (PUC*X*)

PUC*X* sample	ALA–MMT content (wt%)	Modulus (kPa)	ΔModulus[a] (%)	Tensile strength (MPa)	ΔTensile strength[a] (%)	Elongation (%)	ΔElongation[a] (%)
PU	0	2.11	–	1.33	–	631	–
PUC1	1	3.10	47	2.55	92	823	30
PUC3	3	3.26	55	3.32	150	1019	62
PUC5	5	3.27	55	4.01	202	1225	94
PUC7	7	3.30	56	4.63	248	1404	123

[a] The increment compared with the pure PU's data.

of the well-dispersed ALA–MMT in the PU matrix had a remarkable effect on their mechanical properties. Even with 1 wt% of ALA–MMT as the tensile strength, elongation at break and modulus of PUC1 already increased to 92%, 30% and 47%, respectively, and all increased with the increase in the ALA–MMT content in the range of 1–7 wt%. Furthermore, a 248% increase in the tensile strength and a 123% increase in the elongation at break were found for PUC7. The enhancement in the mechanical properties of the as-prepared PU/ALA–MMT nanocomposites is again mainly attributed to the presence of the well-dispersed and highly exfoliated silicate layers, which are chemically linked to the PU matrix through the carboxylic acid group of the reactive swelling agent, ALA.

3.6. Corrosion protection properties of PU/ALA–MMT nanocomposite coatings

The corrosion protection properties of the PU/ALA–MMT nanocomposite coatings on the stainless steel disks (SSDs) were evaluated by the Tafel method, which is one of the best electrochemical techniques to study the corrosion prevention effect of a surface coating on a metal surface according to the values of corrosion potential (E_{corr}), polarization resistance (R_p), corrosion current (I_{corr}), and corrosion rate (R_{corr}) measured after immersion in 5 wt% NaCl solution for 30 min. Fig. 9 shows the Tafel plots for the uncoated, PU-coated, and PU/ALA–MMT-coated SSD samples. As listed in Table 4, the PU/ALA–MMT-coated SSD exhibited higher E_{corr} values than the uncoated SSD (−434 mV), and it increased with an increase in the amount of ALA–MMT clay. The E_{corr} value for the PU-coated SSD was −365 mV, and this increased to −307 mV for PUC1-coated SSD, to −244 mV for PUC3-coated SSD, to −139 mV for PUC5-coated SSD, and to −31 mV for PUC7-coated SSD. Furthermore, the PUC7-coated SSD showed a polarization resistance (R_p) value of 3933 kΩ, which was higher than that for the PU-coated SSD (1552 kΩ), and much higher than that for the SSD (55 kΩ). The corrosion current (I_{corr}) of PUC1-coated SSD (105 nA/cm^2, corresponding to a corrosion rate (R_{corr}) of 7.12×10^{-6} mm/year) was smaller than that of PU-coated SSD (9.43×10^{-6} mm/year), and it decreased gradually with an increase in ALA–MMT loading, revealing that the anti-corrosive property of the PU film was enhanced due to the dispersion of ALA–MMT in the PU matrix. This implies that the PU/ALA–MMT-coated SSDs are more inert toward electrochemical corrosion than the clay-free PU-coated SSD. The enhancement of the corrosive protection effect is attributed to the increase in the tortuosity of the diffusion pathways of O_2 molecules due to the presence of the dispersed silicated nanolayers. Moreover, the PUC7-coated SSD had the highest E_{corr} and R_p, as well as the lowest I_{corr} and R_{corr} among the system. The R_{corr} of the PUC7-coated SSD coupon was 2.01×10^{-6} mm/year, and it was 469% lower than that of the PU-coated SSD, implying that the PUC7 film has the highest anti-corrosive protection on the SSD surface. This is consistent with the XRD results, which suggested that the content of the clay silicate galleries in PUC7 was the highest and most exfoliated, providing the longest tortuosity of the diffusion pathway of O_2 molecules among the as-prepared PU/ALA–MMT-coated SSDs.

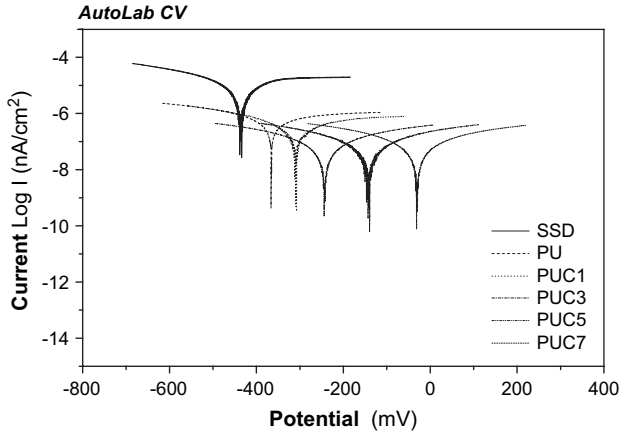

Fig. 9. Tafel plots of PU/ALA–MMT nanocomposites (PUC*X*).

Table 4
Corrosion protection properties of PU/ALA–MMT nanocomposites (PUC*X*)

Composite coated on SSD	Coating thickness (μm)	Electrochemical corrosion measurements			
		E_{corr} (mV)	I_{corr} (nA/cm^2)	R_p (kΩ)	R_{corr} (mm/year)
Uncoated SSD	–	−434	6811	55	2.23×10^{-2}
PU	21	−365	130	1552	9.43×10^{-6}
PUC1	23	−307	105	2083	7.12×10^{-6}
PUC3	22	−244	82	2816	5.77×10^{-6}
PUC5	25	−139	68	3484	4.73×10^{-6}
PUC7	23	−31	55	3933	2.01×10^{-6}

4. Conclusion

In this study, stable de-aggregated solvent-swollen organic modified clay, ALA–MMT, was obtained by modifying the montmorillonite with the swelling agent, ALA, a carboxylic acid group-containing, long-chain-alkylamine. The suspension was prepared by an efficient solvent swelling process using a home-made shaking mixer. The average size of the suspended ALA–MMT particles was reduced to about 155 nm, and the *d*-spacing of the clay layers was expanded from 1.4 nm to about 2.1 nm. A series of PU/ALA–MMT nanocomposites were prepared from the as-prepared solvent-swollen ALA–MMT and PU. The PU/ALA–MMT nanocomposites were confirmed by the XRD diffraction patterns, and the TEM photographs exhibited a highly exfoliated structure even with as high as 7 wt% of ALA–MMT addition, resulting in tremendous reinforcements in their thermal stability, mechanical properties, and anti-corrosion protection as well. In addition, the reinforcements were much greater than the previously reported PU/clay nanocomposites with comparable clay loadings. This is ascribed to the proper dispersion and high exfoliation of the loaded organoclay due to the reactivity of carboxylic acid groups, the long-chain structure of the swelling agent, and the stable de-aggregated solvent-swollen organoclay suspension prepared by the effective solvent swelling process using the shaking mixer.

Acknowledgment

The authors would like to thank the National Science Council of the Republic of China for supporting this research under contract no. 92-2745-M-033-001.

References

[1] Xu R, Manias E, Snyder AJ, Runt J. J Biomed Mater Res 2003;64A(1):114.
[2] Hu Y, Wang S, Ling Z, Zhuang YL, Chen Z, Fan WC. Macromol Mater Eng 2003;288:272.
[3] Wang S, Hu Y. Polym Degrad Stab 2002;77:423.
[4] Tang Y, Hu Y, Wang S, Gui Z, Chen Z, Fan WC. Polym Degrad Stab 2002;78:555.
[5] Giannelis EP. Adv Mater 1996;8:29.
[6] Gilman JW, Jackson CL, Harris Jr R, Morgan AB. Chem Mater 2000;12:1866.
[7] Porter D, Metcalfe E, Thomas MJK. Fire Mater 2000;24:45.
[8] Messersmith PB, Giannelis EP. J Polym Sci Part A Polym Chem 1995;33:1047.
[9] Zhu J, Morgan AB, Lamelas FJ, Wilkie CA. Chem Mater 2001;13:3774.
[10] Ghosh AK, Woo EM. Polymer 2004;45:4749.
[11] Wang MS, Pinnavaia TJ. Chem Mater 1994;6:468.
[12] Messersmith PB, Giannelis EP. Chem Mater 1994;6:1719.
[13] Lan T, Kaviratna PD, Pinnavaia TJ. Chem Mater 1995;7:2144.
[14] Langat J, Bellayer S, Hudrlik P, Hudrlik A, Maupin PH, Gilman JW, et al. Polymer 2006;47:6698.
[15] Chang JH, Park DK, Ihn KJ. J Appl Polym Sci 2002;84:2294.
[16] Tyan HL, Leu CM, Wei KH. Chem Mater 2001;13:222.
[17] Lee MH, Dan CH, Kim JH, Cha J, Kim S, Hwang Y, et al. Polymer 2006;47:4359.
[18] Stadtmueller LM, Ratinac KR, Ringer SP. Polymer 2005;46:9574.
[19] Xu Y, Brittain WJ, Xue CC, Eby RK. Polymer 2004;45:3735.
[20] Tien YI, Wei KH. J Polym Res 2000;7:245.
[21] Chen TK, Tien YI, Wei KH. J Polym Sci Part A Polym Chem 1999;37:2225.
[22] Mariaosaria T, Giuliana G, Vittoria V, Giancarlo G, Stefano R, Euro C. Polymer 2002;43:6147.
[23] Dai X, Xu J, Guo XL, Lu YL, Shen D, Zhao N, et al. Macromolecules 2004;37:5615.
[24] Kim BK, Seo JW, Jeong HM. Eur Polym J 2003;39:85.
[25] Vaia RA, Vasudevan S, Krawiec W, Scanlon LG, Giannelis EP. Adv Mater 1995;7:154.
[26] Tien YI, Wei KH. Macromolecules 2001;34:9045.
[27] Tien YI, Wei KH. J Appl Polym Sci 2002;86:1741.
[28] Choi WJ, Kim SH, Kim YJ, Kim SC. Polymer 2004;45:6045.
[29] Chen-Yang YW, Yang HC, Li GJ, Li YK. J Polym Res 2004;11:275.
[30] Ma J, Zhang S, Qi Z. J Appl Polym Sci 2001;82:1444.
[31] Kim DS, Kim JT, Woo WB. J Appl Polym Sci 2005;96:641.
[32] Song L, Hu Y, Li B, Wang S, Fan W. Int J Polym Anal Charact 2003;8:317.
[33] Solarski S, Benali S, Rochery M, Devaux E, Alexandre M, Monteverde F, et al. J Appl Polym Sci 2005;95:238.
[34] Zhang X, Xu R, Wu Z, Zhou C. Polym Int 2003;52:790.
[35] Chang JH, An YU. J Polym Sci Part B Polym Phys 2002;40:670.
[36] Kitti KS, Sikdar D, Katti DR, Ghosh P, Verma D. Polymer 2006;47:403.